Available online at www.sciencedirect.com
SCIENCE DIRECT®
Journal of Sound and Vibration 278 (2004) 39–62
JOURNAL OF SOUND AND VIBRATION
www.elsevier.com/locate/jsvi

Treatment of singularities in Helmholtz-type equations using the boundary element method

L. Marin[a,*], D. Lesnic[b], V. Mantič[c]

[a] School of the Environment, University of Leeds, Leeds LS2 9JT, UK
[b] Department of Applied Mathematics, University of Leeds, Leeds LS2 9JT, UK
[c] School of Engineering, University of Seville, Camino de los Descubrimientos s/n, Seville E-41902, Spain

Received 12 June 2003; accepted 25 September 2003

Abstract

In many engineering problems, boundaries with sharp corners or abrupt changes in the boundary conditions and/or the material properties give rise to singularities of various types which tend to slow down the rate of convergence with respect to decreasing the mesh size of any standard numerical method used for obtaining the solution. In this paper, in order to develop a method which overcomes this difficulty, the singular solutions of isotropic and anisotropic Helmholtz-type equations with homogeneous Dirichlet and/or Neumann boundary conditions in the neighbourhood of a singular point are derived. The standard boundary element method (BEM) is then modified to take account of the form of singularity, without an appreciable increase in the computational effort and at the same time keeping a uniform discretization. Three examples are carefully investigated and the numerical results presented show an excellent performance of the approach developed.

1. Introduction

In many practical engineering problems governed by elliptic partial differential equations, such as crack initiation and propagation, failure of adhesive joints, edge diffraction, etc., the solution and its derivatives may have unbounded values if the boundary of the solution domain is non-smooth, e.g., sharp re-entrant corners in the boundary, the boundary conditions change abruptly, or there are discontinuities in the material properties. All these situations give rise to singularities of various types and standard numerical methods for solving the boundary value problems (BVPs) in this case exhibit slow convergence and inaccurate approximations to the exact solution

*Corresponding author. Tel.: +44-113-343-6744; fax: +44-113-343-6716.
E-mail address: liviu@env.leeds.ac.uk (L. Marin).

0022-460X/$ - see front matter © 2003 Elsevier Ltd. All rights reserved.
doi:10.1016/j.jsv.2003.09.059

in the neighbourhood of the singularity, see Refs. [1–9]. It is now a classical result, see Ref. [10] and the references given therein, that the singular solution $u^{(S)}$ of an elliptic equation at a corner associated to a singularity exponent λ admits an expansion of the form

$$u^{(S)}(r,\theta)=\sum_{p=0}^{\infty} u_p(r,\theta), \quad u_p(r,\theta)=\sum_{q=0}^{Q} r^{\lambda+p}\log^q r\cdot\phi_{p,q}(\theta), \tag{1}$$

where (r,θ) are the local polar co-ordinates at the corner and $\phi_{p,q}(\theta)$ are smooth angular functions. Here the term u_0 represents the principal term, whilst the remaining terms correspond to the non-principal part of the elliptic operator and of the boundary conditions, and the curvature of the boundary at the corner tip. The singularity exponents λ are defined by the roots of the characteristic equation associated to the local configuration at the corner tip given by the corner geometry, boundary conditions and material properties.

There are important studies regarding the numerical treatment of singularities for BVPs in the literature. Motz [1] has investigated the removal of the singularity for the Laplace and the biharmonic equations using the finite difference method (FDM). Later, Symm [2] and Wait [3] have solved singular direct problems for the Laplace equation by employing the boundary element method (BEM) and the finite element method (FEM), respectively. Modified BEMs that take into account the singularities caused by an abrupt change in the boundary conditions and the presence of a sharp re-entrant corner in the boundary of the solution domain have been developed for the time-dependent diffusion equation and the anisotropic steady state heat conduction problem by Lesnic et al. [4] and Mera et al. [5], respectively. The singular function boundary integral method has been applied for the solution of the Laplace equation in an L-shaped domain by Elliotis et al. [6] who have approximated the solution by the leading terms of the local solution expansion and have weakly enforced the boundary conditions by means of Lagrange multipliers. With respect to singularities in elastostatics, the pioneering theoretical work of Williams [7], who has developed explicit expressions for singular solutions for the problems of single free–free, clamped–clamped and clamped–free isotropic elastic corners, should be mentioned. From the numerous numerical investigations in fracture mechanics, the papers by Portela et al. [8] and Helsing and Jonsson [9] are mentioned who have employed the Williams basis functions in conjunction with the dual BEM and a modified Fredholm second-kind integral together with the Nyström method, respectively, in order to study the behaviour of the stress field in domains with traction–free re-entrant corners.

The Helmholtz equation arises naturally in many physical applications related to wave propagation and vibration phenomena. It is often used to describe the vibration of a structure, see Refs. [11–13], the acoustic cavity problem, see Refs. [14–16], the radiation wave, see Refs. [17,18], and the scattering of a wave, see Refs. [19,20]. Another important application of Helmholtz-type equations is the problem of heat conduction in fins, see e.g., Refs. [21–23].

Many authors have treated singularities occuring in the Helmholtz equation. Time-harmonic waves in a membrane which contains one or more fixed edge stringers or cracks have been investigated by Chen et al. [13] who have employed the dual BEM in order to obtain an efficient solution of the Helmholtz equation in the presence of geometric singularities. Chen and Chen [14] have used the dual integral formulation for the Helmholtz equation to determine the acoustic modes of a two-dimensional cavity with a degenerate boundary. Huang et al. [17] have investigated the electromagnetic field due to a line source radiating in the presence of a

two-dimensional composite wedge made of a number of conducting and dielectric materials by employing the Fourier transform path integral method. A hybrid asymptotic/FEM for computing the acoustic field radiated or scattered by acoustically large objects has been developed by Barbone et al. [20]. Schiff [24] has computed the transverse electric (TE) and transverse magnetic (TM) mode eigenvalues for ridged and other waveguides by using super-elements for the FEM, a refined local mesh and basis functions at the corner tip. The method of the auxiliary mapping, in conjunction with the p-version of the FEM, has been used by Cai et al. [25] and Lucas and Oh [26] in order to remove the pollution effect caused by singularities in the Helmholtz equation. Both Laplace- and Helmholtz-type BVPs with singularities have been considered by Wu and Han [27] who have solved these problems using the FEM and by introducing a sequence of approximations to the boundary conditions at an artificial boundary and then reducing the original problems to BVPs away from the singularities. Xu and Chen [28] have used the FDM and higher order discretized boundary conditions at the edges of perfectly conducting wedges for TE waves to retrieve accurately the field behaviour near a sharp edge.

In the case of the anisotropic Helmholtz equation, the differential operator has the form $K_{ij}\partial_{x_i}\partial_{x_j} + k^2$, where K_{ij} is a symmetric, positive-definite matrix and k is the so-called wave number. The principal and non-principal parts of the Helmholtz operator are defined by the second order differential operator $K_{ij}\partial_{x_i}\partial_{x_j}$ and the zeroth-order operator k^2, respectively. Thus, the singularity exponents and the principal term u_0 in Eq. (1) are independent of k. The singularity exponents and principal terms associated to multi-material corners in the case of anisotropic potential problems, which represent the limiting case with $k = 0$, have been recently investigated in a comprehensive way and the reader is referred to Mantič et al. [29].

An accurate analysis of Helmholtz-type equations in the presence of two-dimensional wedges requires the knowledge of the singular local behaviour of the solution in the neighbourhood of the corner tip in order to improve the accuracy of the numerical solution. The analytical method developed in the present work permits the study and analysis of BVPs with singularities for both the Helmholtz (k real number) and the modified Helmholtz (k imaginary number) equations. Due to the fact that solutions of the two-dimensional Helmholtz equation have a discontinuous limit when $k \to 0$, the case $k = 0$, studied in Refs. [5,29], has been excluded from the scope of the present work. For the sake of brevity, the present paper is based on the closely related paper by Mantič et al. [29], which has allowed several proofs and expressions presented therein to be omitted here and appropriate references to be given. In addition, the present method can be generalized to the wave propagation in elastic isotropic and anisotropic corners. The method proposed in this paper has been implemented numerically by accommodating the standard BEM for the Helmoltz-type equations to take account of the form of the singularity, without appreciably increasing the amount of computation involved, as well as without refining the mesh in the vicinity of the singular point.

2. General solution of Helmholtz-type equations in polar co-ordinates

2.1. Isotropic Helmholtz-type equation

In this section, some well-known results on the solution of the homogeneous Helmholtz-type equation using the separation of variables in polar co-ordinates are revised, and the notation used

in the present work is introduced. If $k = \alpha + i\beta$ is a fixed non-zero complex number ($\alpha, \beta \in \mathbb{R}$) then the isotropic Helmholtz-type equation in a plane domain $\Omega \subset \mathbb{R}^2$ is defined as

$$\Delta u(\mathbf{x}) + k^2 u(\mathbf{x}) = 0, \quad \mathbf{x} \in \Omega, \tag{2}$$

where k is called the wave number when it is real and positive.

Let the polar co-ordinate system (r, θ) be defined in the usual way with respect to the Cartesian co-ordinates $(x_1, x_2) = (r\cos\theta, r\sin\theta)$. For $r > 0$, Eq. (2), written in polar co-ordinates takes the following form:

$$(\partial_r^2 + r^{-1}\partial_r + r^{-2}\partial_\theta^2 + k^2)u(r, \theta) = 0. \tag{3}$$

If it is assumed that the solution in Ω of Eq. (2) can be written using the separation of variables

$$u(r, \theta) = f(r)g(\theta), \tag{4}$$

then the Helmholtz-type Eq. (2) recasts as

$$(f''(r) + r^{-1}f'(r) + k^2 f(r))g(\theta) + r^{-2}f(r)g''(\theta) = 0. \tag{5}$$

If $f(r)g(\theta) \neq 0$ then the following ratio must be a constant, defined here as λ^2:

$$\frac{f''(r) + r^{-1}f'(r) + k^2 f(r)}{r^{-2}f(r)} = -\frac{g''(\theta)}{g(\theta)} = \lambda^2, \tag{6}$$

yielding the following linear homogeneous ordinary differential equations in r and θ, respectively:

$$f''(r) + r^{-1}f'(r) + \left(k^2 - \frac{\lambda^2}{r^2}\right)f(r) = 0, \tag{7}$$

$$g''(\theta) + \lambda^2 g(\theta) = 0. \tag{8}$$

For a given value of λ, the general solution of Eq. (8) can be written as

$$g(\theta) = a_c \cos(\lambda\theta) + a_s \sin(\lambda\theta), \tag{9}$$

where a_c and a_s are constants. The general solution of Eq. (7) can be written using the linearly independent Bessel functions of the first kind, J_λ, and the second kind (also called Weber or Neumann functions), N_λ, as

$$f_\lambda(kr) = c_1 J_\lambda(kr) + c_2 N_\lambda(kr), \tag{10}$$

where c_1 and c_2 are constants. In the analysis of the solution u the following asymptotic expansions for complex $z \to 0$ are useful:

$$J_\lambda(z) \cong \frac{1}{\Gamma(\lambda+1)}\left(\frac{z}{2}\right)^\lambda (\mathrm{Re}\,\lambda \geqslant 0), \quad N_0(z) \cong \frac{2}{\pi}\ln z, \quad N_\lambda(z) \cong -\frac{\Gamma(\lambda)}{\pi}\left(\frac{2}{z}\right)^\lambda (\mathrm{Re}\ \lambda > 0). \tag{11}$$

Hence, the general solution of Eq. (2) in form (4) can be written as

$$u(r, \theta) = (c_1 J_\lambda(kr) + c_2 N_\lambda(kr))(a_c \cos(\lambda\theta) + a_s \sin(\lambda\theta)). \tag{12}$$

2.2. Anisotropic Helmholtz-type equation

In this section, the general solution of the anisotropic Helmholtz-type equation is obtained following an approach developed by Mantič et al. [29]. The approach is based on a change of

variables, which transforms the anisotropic Helmholtz-type equation to the canonical form with the same wave number, and on a subsequent application of the results from the previous section. It has to be stressed that the final solution expressed in polar co-ordinates defined in the anisotropic plane does not represent the solution corresponding to the separation of variables, as given by Eq. (4), due to the presence of the angular variable in the argument of the Bessel function, a fact that does not happen in the case of an isotropic medium.

Let $\mathbf{K}$ be a constant, symmetric and positive-definite matrix which defines the anisotropic material properties in the domain $\Omega \subset \mathbb{R}^2$. Then, the anisotropic Helmholtz-type equation recasts as

$$K_{ij}\partial_{x_i}\partial_{x_j}u(\mathbf{x}) + k^2 u(\mathbf{x}) = 0, \quad \mathbf{x} \in \Omega. \tag{13}$$

Let the matrix $\mathbf{L}$ be defined as a factor in the symmetric decomposition of the inverse of the matrix $\mathbf{K}$, i.e.,

$$\mathbf{K}^{-1} = \mathbf{L}^{\mathrm{T}}\mathbf{L}, \quad \mathbf{K} = \mathbf{L}^{-1}(\mathbf{L}^{-1})^{\mathrm{T}}. \tag{14}$$

It should be noted that the matrix $\mathbf{L}$ is not uniquely defined, see Ref. [29] for a discussion of the usual definitions of $\mathbf{L}$ in the literature. Without any loss of generality it can be assumed that the determinant $|\mathbf{L}|$ is positive. If the transformation of co-ordinates

$$\tilde{x}_i = L_{ij}x_j, \tag{15}$$

is considered then the general solution of Eq. (13) in Ω is given by the general solution $\tilde{u}(\tilde{\mathbf{x}})$ of the isotropic (modified) Helmholtz-type equation

$$\Delta\tilde{u}(\tilde{\mathbf{x}}) + k^2\tilde{u}(\tilde{\mathbf{x}}) = 0, \tag{16}$$

in the transformed domain $\tilde{\Omega} = \mathbf{L}\Omega \subset \mathbb{R}^2$ via the following representation:

$$u(\mathbf{x}) = \tilde{u}(\mathbf{L}\mathbf{x}). \tag{17}$$

The proof of the above statement follows directly from the following relation, see Refs. [29,30]:

$$K_{ij}\partial_{x_i}\partial_{x_j}u(\mathbf{x}) = \Delta\tilde{u}(\tilde{\mathbf{x}}). \tag{18}$$

Consider a curve $\Gamma \subset \bar{\Omega}$ and denote by $\mathbf{n}(\mathbf{x})$ the unit normal vector at $\mathbf{x} \in \Gamma$ then the normal flux through Γ at $\mathbf{x}$ is given by the conormal derivative

$$q(\mathbf{x}) \equiv \partial_\nu u(\mathbf{x}) = n_i(\mathbf{x})K_{ij}\partial_{x_j}u(\mathbf{x}). \tag{19}$$

The unit normal vector $\tilde{\mathbf{n}}(\tilde{\mathbf{x}})$ to the transformed curve $\tilde{\Gamma} = \mathbf{L}\Gamma$ at $\tilde{\mathbf{x}}$ is expressed as, see Refs. [29,30]

$$\tilde{\mathbf{n}}(\tilde{\mathbf{x}}) = \frac{(\mathbf{L}^{-1})^{\mathrm{T}}\mathbf{n}(\mathbf{x})}{n_K(\mathbf{x})}, \quad \text{where} \quad n_K(\mathbf{x}) = \sqrt{\mathbf{n}(\mathbf{x})^{\mathrm{T}}\mathbf{K}\mathbf{n}(\mathbf{x})}, \tag{20}$$

whilst the transformed normal flux through $\tilde{\Gamma}$ at $\tilde{\mathbf{x}}$ associated to problem (16) is given by

$$\tilde{q}(\tilde{\mathbf{x}}) = \tilde{\mathrm{n}}_i(\tilde{\mathbf{x}})\partial_{\tilde{x}_i}\tilde{u}(\tilde{\mathbf{x}}) = \frac{q(\mathbf{x})}{n_K(\mathbf{x})}. \tag{21}$$

Consider now the polar co-ordinate system $(\tilde{r}, \tilde{\theta})$ defined in the transformed plane in the usual way, i.e. $(\tilde{x}_1, \tilde{x}_2) = (\tilde{r}\cos\tilde{\theta}, \tilde{r}\sin\tilde{\theta})$. Starting from relation (15), it can be easily shown that

$$\tilde{r} = \tilde{r}(r, \theta) = r\rho(\theta), \quad \tilde{\theta} = \tilde{\theta}(\theta), \tag{22}$$

where the radial scaling factor $\rho(\theta)$ is a smooth periodic function with the period π given by, see Ref. [29],

$$\rho(\theta) = \sqrt{\mathbf{e}(\theta)^{\mathrm{T}}\mathbf{K}^{-1}\mathbf{e}(\theta)} > 0, \tag{23}$$

and $\mathbf{e}(\theta) = (\cos\theta, \sin\theta)$. It should be noted that in the particular case of an isotropic material $\rho(\theta)$ is constant. Although the value of the transformed angle $\tilde{\theta} = \tilde{\theta}(\theta)$ depends on the particular choice of $\mathbf{L}$, its derivative is independent of this choice and it is given by, see Ref. [29],

$$\frac{\mathrm{d}\tilde{\theta}}{\mathrm{d}\theta} = \frac{1}{\sqrt{|\mathbf{K}|}\rho^2(\theta)}. \tag{24}$$

Substituting expression (12) into representation (17), the general solution of the anisotropic Helmholtz-type equation (13) is obtained in the form

$$u(r,\theta) = c_1 \mathrm{J}_\lambda(kr\rho(\theta)) + c_2 \mathrm{N}_\lambda(kr\rho(\theta))\{a_c \cos(\lambda\tilde{\theta}(\theta)) + a_s \sin(\lambda\tilde{\theta}(\theta))\}. \tag{25}$$

3. Corner singularities for Helmholtz-type equations

In this section, a procedure applied by Mantič et al. [29] is generalized in order to obtain the singularity exponents and the singular solutions of Helmholtz-type equations for anisotropic materials containing corners.

Let $\Omega \subset \mathbb{R}^2$ denote an anisotropic homogeneous wedge domain of interior angle ω, $0 < \omega \leqslant 2\pi$, with the tip at the origin of co-ordinates and determined by two straight edges of angles θ_0 and θ_1, respectively, where $\omega = \theta_1 - \theta_0$. Thus, $\Omega = \{\mathbf{x} \in \mathbb{R}^2 | 0 < r < R(\theta), \theta_0 < \theta < \theta_1\}$, where $R(\theta)$ is either a bounded continuous function or infinity. The value of the angle $\tilde{\omega}$ of the transformed wedge domain $\tilde{\Omega} = \mathbf{L}\Omega$ is given by (see Ref. [29]),

$$\tilde{\omega} = \tilde{\theta}(\theta_1) - \tilde{\theta}(\theta_0) = \int_{\theta_0}^{\theta_1} \frac{\mathrm{d}\tilde{\theta}}{\mathrm{d}\theta}\,\mathrm{d}\theta = \pi + \mathrm{sgn}(\omega - \pi)\arccos\left(-\frac{\mathbf{e}^{\mathrm{T}}(\theta_1)\mathbf{K}^{-1}\mathbf{e}(\theta_0)}{\rho(\theta_1)\rho(\theta_0)}\right), \tag{26}$$

where sgn denotes the signum function. From relation (26), it follows that $\tilde{\omega} = \omega$ for the limit values $\omega = 0$ or $\omega = 2\pi$ and also for $\omega = \pi$. If $\omega = \pi/2$ or $\omega = 3\pi/2$ and the wedge faces are parallel to the orthotropy axes of the material then $\tilde{\omega} = \omega$ as well.

In what follows, the BVP in Ω defined by Eq. (13) is considered and homogeneous Neumann or Dirichlet boundary conditions prescribed along the wedge edges. If it is assumed that $\mathrm{Re}\,\lambda \geqslant 0$, then on taking into account relation (11) with $z = kr\rho(\theta)$ as $r \to 0_+$ and the finite character of u in a wedge tip neighbourhood, $c_2 = 0$ is obtained in Eq. (25). Hence the basis function of singular solutions to the above BVP obtained from expression (25) can be written in the general form as

$$u^{(S)}(r,\theta) = \mathrm{J}_\lambda(kr\rho(\theta))\{a_c \cos(\lambda\tilde{\theta}(\theta)) + a_s \sin(\lambda\tilde{\theta}(\theta))\}, \tag{27}$$

where λ is referred to as the singularity exponent.

The normal flux through a straight radial line defined by an angle θ and associated to the normal vector $\mathbf{n}(\theta) = (-\sin\theta, \cos\theta)$ is given, in view of (21), by

$$q^{(S)}(r,\theta) = \tilde{q}^{(S)}(\tilde{r},\tilde{\theta}) n_K(\theta), \quad \text{where} \quad \tilde{q}^{(S)}(\tilde{r},\tilde{\theta}) = \tilde{r}^{-1}\partial_{\tilde{\theta}}\tilde{u}^{(S)}(\tilde{r},\tilde{\theta}), \tag{28}$$

and, by using Eqs. (20_2) and (23), it can be shown that

$$n_K(\theta) = \sqrt{\mathbf{n}^{\mathrm{T}}(\theta)\mathbf{K}\mathbf{n}(\theta)} = \sqrt{|\mathbf{K}|}\rho(\theta). \tag{29}$$

For the sake of convenience, solution (27) and flux (28) are re-written, respectively, as

$$u^{(S)}(r,\theta) = \mathrm{J}_\lambda(kr\rho(\theta))\{a_c\cos(\lambda(\tilde{\theta}(\theta) - \tilde{\theta}(\theta_0))) + a_s\sin(\lambda(\tilde{\theta}(\theta) - \tilde{\theta}(\theta_0)))\}, \tag{30}$$

$$q^{(S)}(r,\theta) = \frac{\lambda\sqrt{|\mathbf{K}|}}{r}\mathrm{J}_\lambda(kr\rho(\theta))\{-a_c\sin(\lambda(\tilde{\theta}(\theta) - \tilde{\theta}(\theta_0))) + a_s\cos(\lambda(\tilde{\theta}(\theta) - \tilde{\theta}(\theta_0)))\}. \tag{31}$$

Possible values of λ depend on the boundary conditions prescribed at the wedge edges. In this study, four configurations of homogeneous Neumann (N) and Dirichlet (D) boundary conditions at the wedge edges applied to expressions (30) and (31) are considered. Look at the conditions which allow a nontrivial solution of the resulting system of equations under the assumption $\mathrm{Re}\,\lambda \geqslant 0$.

Case I: N–N wedge

$$q^{(S)}(r,\theta_0) = q^{(S)}(r,\theta_1) = 0 \Rightarrow a_s = 0 \text{ and } \sin\lambda\tilde{\omega} = 0 \Rightarrow \lambda = l\frac{\pi}{\tilde{\omega}} \quad \text{for } l \in \mathbb{N}\cup\{0\}, \tag{32}$$

where N is the set of positive integers.

Case II: D–D wedge

$$u^{(S)}(r,\theta_0) = u^{(S)}(r,\theta_1) = 0 \Rightarrow a_c = 0 \text{ and } \sin\lambda\tilde{\omega} = 0 \Rightarrow \lambda = l\frac{\pi}{\tilde{\omega}} \quad \text{for } l \in \mathbb{N}. \tag{33}$$

Case III: N–D wedge

$$q^{(S)}(r,\theta_0) = u^{(S)}(r,\theta_1) = 0 \Rightarrow a_s = 0 \text{ and } \cos\lambda\tilde{\omega} = 0 \Rightarrow \lambda = \left(l - \frac{1}{2}\right)\frac{\pi}{\tilde{\omega}} \quad \text{for } l \in \mathbb{N}. \tag{34}$$

Case IV: D–N wedge

$$u^{(S)}(r,\theta_0) = q^{(S)}(r,\theta_1) = 0 \Rightarrow a_c = 0 \text{ and } \cos\lambda\tilde{\omega} = 0 \Rightarrow \lambda = \left(l - \frac{1}{2}\right)\frac{\pi}{\tilde{\omega}} \quad \text{for } l \in \mathbb{N}. \tag{35}$$

It can be noticed that the above singularity exponents λ are real and simple, and they coincide in cases I and II, and III and IV, respectively. Using the above results, the general asymptotic expansions for the singular solution of the anisotropic Helmholtz-type equation for a single wedge corresponding to homogeneous Neumann and Dirichlet boundary conditions on the wedge edges are obtained in the following form:

Case I: N–N wedge

$$u^{(S)}(r,\theta) = \sum_{l=0}^{\infty} a_l u_l^{(S)}(r,\theta) = \sum_{l=0}^{\infty} a_l \mathrm{J}_{l\frac{\pi}{\tilde{\omega}}}(kr\rho(\theta))\cos\left\{l\frac{\pi}{\tilde{\omega}}(\tilde{\theta}(\theta) - \tilde{\theta}(\theta_0))\right\}. \tag{36}$$

Case II: D–D wedge

$$u^{(S)}(r,\theta) = \sum_{l=1}^{\infty} a_l u_l^{(S)}(r,\theta) = \sum_{l=1}^{\infty} a_l \mathrm{J}_{l\frac{\pi}{\tilde{\omega}}}(kr\rho(\theta))\sin\left\{l\frac{\pi}{\tilde{\omega}}(\tilde{\theta}(\theta) - \tilde{\theta}(\theta_0))\right\}. \tag{37}$$

Case III: N–D wedge

$$u^{(S)}(r,\theta)=\sum_{l=1}^{\infty}a_l u_l^{(S)}(r,\theta)=\sum_{l=1}^{\infty}a_l \mathrm{J}_{(l-1/2)\pi/\tilde{\omega}}(kr\rho(\theta))\cos\left\{\left(l-\frac{1}{2}\right)\frac{\pi}{\tilde{\omega}}(\tilde{\theta}(\theta)-\tilde{\theta}(\theta_0))\right\}. \tag{38}$$

Case IV: D–N wedge

$$u^{(S)}(r,\theta)=\sum_{l=1}^{\infty}a_l u_l^{(S)}(r,\theta)=\sum_{l=1}^{\infty}a_l \mathrm{J}_{(l-\frac{1}{2})\frac{\pi}{\tilde{\omega}}}(kr\rho(\theta))\sin\left\{\left(l-\frac{1}{2}\right)\frac{\pi}{\tilde{\omega}}(\tilde{\theta}(\theta)-\tilde{\theta}(\theta_0))\right\}. \tag{39}$$

4. Modified boundary element method

Consider a two-dimensional bounded domain Ω with a piecewise smooth boundary $\partial\Omega$ which contains a singularity at the origin $O=(0,0)$ that may be caused by a change in the boundary conditions at the origin and/or a re-entrant corner at the origin. For the simplicity of the following explanations, it is assumed that the singularity point is located at the intersection of the Dirichlet and Neumann boundary parts, see Fig. 1, although the method presented herein can easily be extended to other local configurations or boundary conditions. Hence the problem to be solved recasts as

$$\begin{cases} K_{ij}\partial_{x_i}\partial_{x_j}u(\mathbf{x})+k^2u(\mathbf{x})=0, & \mathbf{x}\in\Omega,\\ u(\mathbf{x})=\tilde{u}(\mathbf{x}), & \mathbf{x}\in\Gamma_u,\\ q(\mathbf{x})\equiv\partial_\nu u(\mathbf{x})=\tilde{q}(\mathbf{x}), & \mathbf{x}\in\Gamma_q, \end{cases} \tag{40}$$

where $\bar{\Gamma}_u\cup\bar{\Gamma}_q=\partial\Omega$, $\Gamma_u,\Gamma_q\neq\emptyset$, $\Gamma_u\cap\Gamma_q=\emptyset$, $O\in\bar{\Gamma}_u\cap\bar{\Gamma}_q$, $\tilde{u}$ and $\tilde{q}$ are the prescribed boundary potential solution and flux, respectively, and we denote the closure of a set by an overbar.

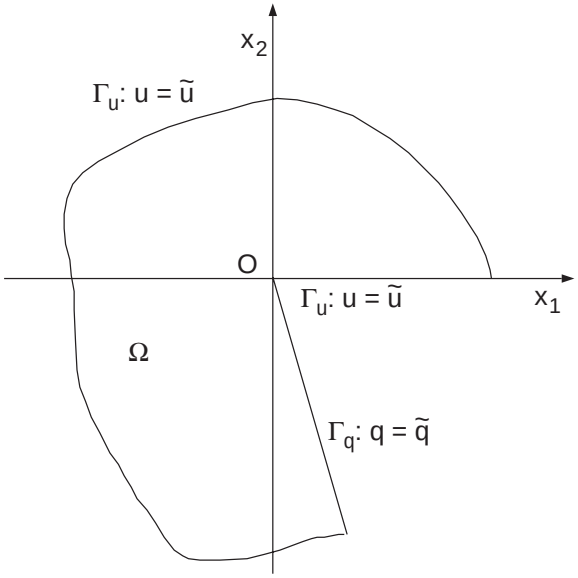

Fig. 1. A schematic diagram of the domain Ω, the singularity point O and the boundary conditions.

In order to avoid numerical difficulties arising from the presence of the singularity in the potential solution at O, it is convenient to modify the original problem before it is solved by the BEM. Due to the linearity of the Helmholtz operator and the boundary conditions, the superposition principle is valid and the potential solution u and the flux q can be written as

$$u(\mathbf{x}) = (u(\mathbf{x}) - u^{(S)}(\mathbf{x})) + u^{(S)}(\mathbf{x}) = u^{(R)}(\mathbf{x}) + u^{(S)}(\mathbf{x}), \quad \mathbf{x} \in \bar{\Omega} = \Omega \cup \partial\Omega,$$

$$q(\mathbf{x}) = (q(\mathbf{x}) - q^{(S)}(\mathbf{x})) + q^{(S)}(\mathbf{x}) = q^{(R)}(\mathbf{x}) + q^{(S)}(\mathbf{x}), \quad \mathbf{x} \in \bar{\Omega} = \Omega \cup \partial\Omega, \tag{41}$$

where $u^{(S)}(\mathbf{x})$ is a particular singular potential solution of the original problem (40) which satisfies the corresponding homogeneous boundary conditions on the parts of the boundary containing the singularity point O and $q^{(S)}(\mathbf{x}) \equiv \partial_v u^{(S)}(\mathbf{x})$ is its conormal derivative. If appropriate functions are chosen for the singular potential solution and its conormal derivative then the numerical analysis can be carried out for the regular potential solution $u^{(R)}(\mathbf{x})$ and its conormal derivative $q^{(R)}(\mathbf{x}) \equiv \partial_v u^{(R)}(\mathbf{x})$ only. In terms of the regular potential solution $u^{(R)}(\mathbf{x})$, the original problem (40) becomes

$$\begin{cases} K_{ij}\partial_{x_i}\partial_{x_j}u^{(R)}(\mathbf{x}) + k^2 u^{(R)}(\mathbf{x}) = 0, & \mathbf{x} \in \Omega, \\ u^{(R)}(\mathbf{x}) = \tilde{u}(\mathbf{x}) - u^{(S)}(\mathbf{x}), & \mathbf{x} \in \Gamma_u, \\ q^{(R)}(\mathbf{x}) \equiv \partial_v u^{(R)}(\mathbf{x}) = \tilde{q}(\mathbf{x}) - q^{(S)}(\mathbf{x}), & \mathbf{x} \in \Gamma_q. \end{cases} \tag{42}$$

The modified boundary conditions (42_2) and (42_3) introduce additional unknowns into the problem, which are the constants of the particular potential solution used to represent the singular potential solution. It should be noted that these constants are similar to the stress intensity factors corresponding to an analogous problem for the Lamé system and, in what follows, they will be referred to as "flux intensity factors". Since the flux intensity factors are unknown at this stage of the problem, they become primary unknowns.

In order to obtain a unique potential solution of the regular problem (42), it is necessary to specify additional constraints which must be as many as the number of the unknown flux intensity factors, i.e., one for each singular solution/eigenfunction included in the analysis. These extra conditions must be applied in such a way that the cancellation of the singularity in the regular potential solution is ensured. This is achieved by constraining the regular potential solution and/or its conormal derivative directly in a neighbourhood of the singularity point O

$$u^{(R)}(\mathbf{x}) = 0, \quad \mathbf{x} \in \Gamma_q \cap B(O;\varepsilon) \quad \text{and/or} \quad q^{(R)}(\mathbf{x}) = 0, \quad \mathbf{x} \in \Gamma_u \cap B(O;\varepsilon), \tag{43}$$

where $B(O;\varepsilon) = \left\{ \mathbf{x} = (x_1, x_2) \in \mathbb{R}^2 | \sqrt{x_1^2 + x_2^2} < \varepsilon \right\}$ and $\varepsilon > 0$ is sufficiently small.

For example, for problem (42) the singular potential solution and its normal derivative are expressed, in terms of the polar co-ordinates (r, θ), as

$$u^{(S)}(\mathbf{x}) \equiv u^{(S)}(r,\theta) = \sum_{l=0}^{L} a_l u_l^{(S)}(r,\theta), \quad q^{(S)}(\mathbf{x}) \equiv q^{(S)}(r,\theta) = \sum_{l=0}^{L} a_l q_l^{(S)}(r,\theta), \tag{44}$$

respectively, where $u_l^{(S)}(r,\theta)$ is given by Eq. (39), $q_l^{(S)}(r,\theta)$ is obtained by taking the conormal derivative of $u_l^{(S)}(r,\theta)$, a_l, $l = 1, \ldots, L$, are the unknown flux intensity factors and the following convention has been made $u_0^{(S)}(r,\theta) \equiv 0$ and $q_0^{(S)}(r,\theta) \equiv 0$.

The Helmholtz-type Eq. (42_1) can also be formulated in integral form, see Refs. [31,32]

$$c(\mathbf{x})u^{(R)}(\mathbf{x}) + \int_{\partial\Omega} \partial_{v(\mathbf{y})} E(\mathbf{x},\mathbf{y}) u^{(R)}(\mathbf{y})\, \mathrm{d}\Gamma(\mathbf{y}) = \int_{\partial\Omega} E(\mathbf{x},\mathbf{y}) q^{(R)}(\mathbf{y})\, \mathrm{d}\Gamma(\mathbf{y}), \quad \mathbf{x}\in\bar{\Omega}, \tag{45}$$

where the first integral is considered in the sense of the Cauchy principal value, $c(\mathbf{x}) = 1$ for $\mathbf{x}\in\Omega$, $c(\mathbf{x}) = \frac{1}{2}$ for $\mathbf{x}$ at smooth parts of $\partial\Omega$ and an explicit expression of $c(\mathbf{x})$ for a corner point $\mathbf{x}\in\partial\Omega$ can be taken from Mantič and París [30], and E is the fundamental solution for the Helmholtz-type equation, which in two-dimensions is given by

$$E(\mathbf{x},\mathbf{y}) = \frac{\mathrm{i}}{4\sqrt{|\mathbf{K}|}} H_0^{(1)}(kR), \quad R = \sqrt{(\mathbf{x}-\mathbf{y})^{\mathrm{T}}\mathbf{K}^{-1}(\mathbf{x}-\mathbf{y})}, \tag{46}$$

with $\mathrm{H}_0^{(1)}$ the Hankel function of order zero of the first kind. It should be noted that the BVPs for Helmholtz-type equations are not always well-posed, in the sense that the integral equation (45) does not necessarily have a unique solution for all wave numbers k, see Ref. [31]. More specifically, the eigenvalues of the Laplacian operator need to be removed in order for the BVPs associated with Helmholtz-type equations to be well-posed and, consequently, have a unique solution. However, the wave numbers k for which the solution of the integral equation (45) is not unique have been avoided for the examples presented and analyzed in the next section. A BEM with constant boundary elements, see e.g. Refs. [33,34], is used in order to discretize uniformly the problem given by the system of linear equations (42). If the boundaries Γ_u and Γ_q are uniformly discretized into N_1 and N_2 constant boundary elements, respectively, such that $N = N_1 + N_2$, then on applying (45) at each node on $\partial\Omega$ and using the boundary conditions (42_2) and (42_3), the following relation is arrived at

$$-\sum_{j=1}^{N_1} B_{ij} q_j^{(R)} + \sum_{j=N_1+1}^{N} A_{ij} u_j^{(R)} = -\sum_{j=1}^{N_1} A_{ij}\left(\tilde{u}_j - \sum_{l=1}^{L} a_l u_{lj}^{(S)}\right) + \sum_{j=N_1+1}^{N} B_{ij}\left(\tilde{q}_j - \sum_{l=1}^{L} a_l q_{lj}^{(S)}\right), \tag{47}$$

where $\boldsymbol{A} = (A_{ij})_{1\leqslant i,j\leqslant N}$ and $\boldsymbol{B} = (B_{ij})_{1\leqslant i,j\leqslant N}$ are matrices which depend solely on the discretisation of the boundary $\partial\Omega$ and the material parameters. Eq. (47) represents a system of N linear algebraic equations for $(N+L)$ unknowns, namely the discretised fluxes $q_j^{(R)}$, $j = 1,\ldots,N_1$, and solutions $u_j^{(R)}$, $j = N_1+1,\ldots,N$, as well as the intensity factors a_l, $l = 1,\ldots,L$, which can be recast as

$$\begin{aligned} &-\sum_{j=1}^{N_1} B_{ij} q_j^{(R)} + \sum_{j=N_1+1}^{N} A_{ij} u_j^{(R)} + \sum_{l=1}^{L} a_l\left(-\sum_{j=1}^{N_1} A_{ij} u_{lj}^{(S)} + \sum_{j=N_1+1}^{N} B_{ij} q_{lj}^{(S)}\right) \\ &\quad = -\sum_{j=1}^{N_1} A_{ij}\tilde{u}_j + \sum_{j=N_1+1}^{N} B_{ij}\tilde{q}_j, \quad i\in\{1,\ldots,N\}. \end{aligned} \tag{48}$$

Since system (48) is underdetermined, it is completed by L more equations which represent the discretised versions of relation (43), i.e.,

$$u_{N_1+j}^{(R)} = 0, \quad j\in\{1,\ldots,L\}, \quad \text{or } q_{N_1+1-j}^{(R)} = 0, \quad j\in\{1,\ldots,L\}, \text{ or}$$

$$u_{N_1+(j+1)/2}^{(R)} = 0, \quad j\in\{1,\ldots,L\}, \quad j \text{ odd, and } q_{N_1+1-j/2}^{(R)} = 0, \quad j\in\{1,\ldots,L\}, \quad j \text{ even} \tag{49}$$

with the mention that in Eq. (49) the singular point O is located between the nodes N_1 and (N_1+1).

5. Numerical results and discussion

In this section, the numerical results obtained using the modified BEM proposed in Section 4 are illustrated by considering the following examples for both the isotropic Helmholtz and the isotropic modified Helmholtz equations containing singularities:

Example 1. Consider the following mixed BVP in the rectangle $\Omega=(-1,1)\times(0,1)$, see Ref. [26] and Fig. 2(a),

$$\begin{cases} \Delta u(\mathbf{x})-u(\mathbf{x})=0, & \mathbf{x}=(x_1,x_2)\in\Omega,\\ q(\mathbf{x})\equiv\partial_n u(\mathbf{x})=0, & \mathbf{x}=(x_1,x_2)\in\Gamma_q=(0,1)\times\{0\},\\ u(\mathbf{x})=r^{-1/2}\sinh(r)\cos\left(\theta/2\right), & \mathbf{x}=(x_1,x_2)\in\Gamma_u=\partial\Omega\backslash\Gamma_q. \end{cases} \tag{50}$$

This problem has a singularity at the origin $O=(0,0)$ and its analytical solution is given by

$$u^{(an)}(r,\theta)=r^{-1/2}\sinh(r)\cos(\theta/2),\quad (r,\theta)\in\Omega. \tag{51}$$

Example 2. Let $\Omega=(-1,1)\times(0,1)\cup(-1,0)\times(-1,0]$ be an L-shaped domain and consider the following Dirichlet BVP for the modified Helmholtz equation in Ω, see Ref. [27] and Fig. 2(b),

$$\begin{cases} \Delta u(\mathbf{x})-u(\mathbf{x})=0, & \mathbf{x}=(x_1,x_2)\in\Omega,\\ u(\mathbf{x})=u^{(an)}(\mathbf{x}), & \mathbf{x}=(x_1,x_2)\in\Gamma_u=\partial\Omega, \end{cases} \tag{52}$$

where

$$u^{(an)}(r,\theta)=u_1^{(S)}(r,\theta)-1.30\ u_2^{(S)}(r,\theta)-1.70\ u_4^{(S)}(r,\theta),\quad (r,\theta)\in\Omega \tag{53}$$

is the exact solution of problem (52) with $u_l^{(S)}(r,\theta)$, $l=1,2,4$, given by relation (37).

Example 3. Let Ω be the same as in the previous example, see Fig. 2(b), and consider the following Dirichlet BVP for the Helmholtz equation in the domain Ω:

$$\begin{cases} \Delta u(\mathbf{x})+u(\mathbf{x})=0, & \mathbf{x}=(x_1,x_2)\in\Omega,\\ u(\mathbf{x})=u^{(\mathrm{an})}(\mathbf{x}), & \mathbf{x}=(x_1,x_2)\in\Gamma_u=\partial\Omega, \end{cases} \tag{54}$$

where

$$u^{(\mathrm{an})}(r,\theta)=u_1^{(S)}(r,\theta)-1.30u_2^{(S)}(r,\theta)-1.70u_4^{(S)}(r,\theta),\quad (r,\theta)\in\Omega \tag{55}$$

is the exact solution of problem (54) with $u_l^{(S)}(r,\theta)$, $l=1,2,4$, given by relation (37).

The numerical results presented in this section have been obtained using a uniform discretisation of the boundary $\partial\Omega$ with $N=120$ and 160 constant boundary elements for Example 1 and Examples 2 and 3, respectively. These values have been found sufficiently large such that any further refinement of the mesh size did not significantly improve the accuracy of the numerical

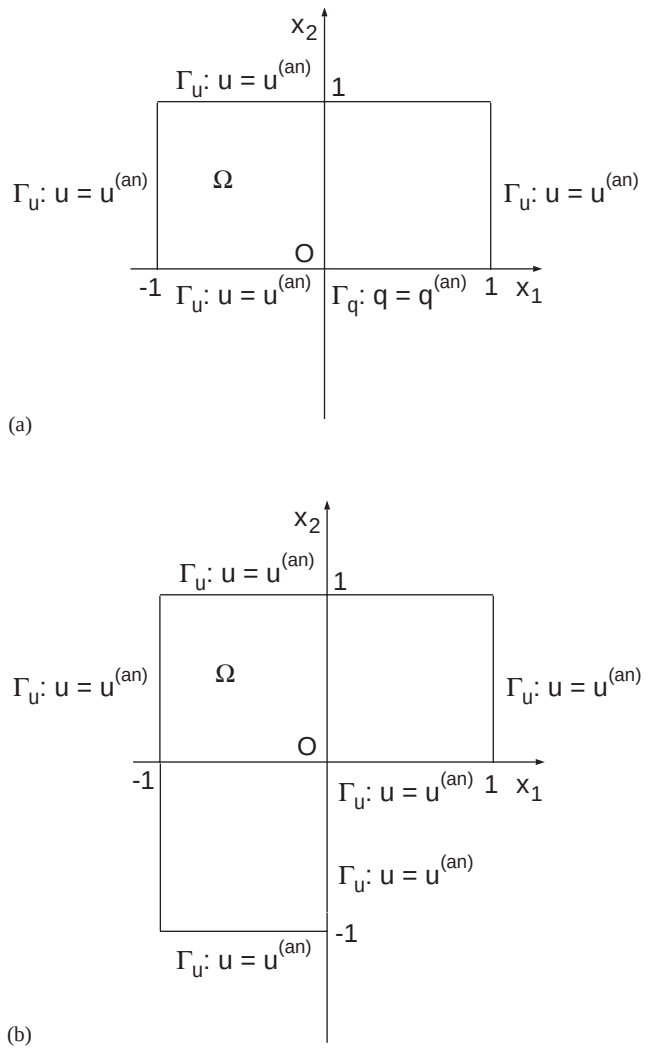

Fig. 2. The geometry of the domain Ω and the boundary conditions for the boundary value problems corresponding to (a) Example 1, and (b) Examples 2 and 3, respectively.

results. In addition, in what follows, denote by $u_L^{(num)}$ and $q_L^{(num)}$ the numerical potential solution and flux, respectively, which are obtained by subtracting the first corresponding L singular potential solutions/eigenvectors

$$u_L^{(num)}(\mathbf{x}) = u_L^{(R)}(\mathbf{x}) + u_L^{(S)}(\mathbf{x}) = u_L^{(R)}(\mathbf{x}) + \sum_{l=0}^{L} a_l u_l^{(S)}(r,\theta), \quad \mathbf{x} \in \bar{\Omega} = \Omega \cup \partial\Omega,$$

$$q_L^{(num)}(\mathbf{x}) = q^{(R)}(\mathbf{x}) + q^{(S)}(\mathbf{x}) = q^{(R)}(\mathbf{x}) + \sum_{l=0}^{L} a_l q_l^{(S)}(r,\theta), \quad \mathbf{x} \in \bar{\Omega} = \Omega \cup \partial\Omega \tag{56}$$

with the convention that when $L = 0$ then the numerical potential solution and flux are obtained using the standard BEM, i.e., without removing the singularity.

The first example investigated contains a singularity at the boundary point $O = (0, 0)$ where there is a change in the boundary conditions. It should be noted that this singularity is of a form which is similar to the case of a sharp re-entrant corner of angle $\omega = 2\pi$. This may be seen by extending the domain $\Omega = (-1, 1) \times (0, 1)$ using symmetry with respect to the x_1-axis. In this way, a problem is obtained for a square domain and a slit, namely $\tilde{\Omega} = (-1, 1) \times (-1, 1) \backslash [0, 1] \times \{0\}$ with zero flux boundary conditions along the slit $[0, 1] \times \{0\}$ and Dirichlet conditions on the remaining boundary of $\tilde{\Omega}$. This problem may also be treated by considering the domain $\tilde{\Omega}$ described above with the mention that the singular eigenvectors (36) corresponding to Neumann–Neumann boundary conditions along the slit must be used. However, the original domain Ω and the mixed boundary conditions described in Eq. (50) have been considered in our analysis, i.e., $\omega = \pi$.

Figs. 3(a) and (b) present the numerical potential solution on the boundary $(0, 1) \times \{0\}$ and flux on the boundary $(-1, 0) \times \{0\}$, respectively, obtained for Example 1 when the standard and the modified BEM are used, in comparison with their analytical values. From these figures it can be seen that the numerical potential solution and flux do not approximate accurately their analytical values in the neighbourhood of the singular point $O = (0, 0)$ when no singular potential solutions are subtracted, i.e., $L = 0$, with the mention that the numerical flux has an oscillatory behaviour in the vicinity of the singularity. Once the modified BEM described in Section 4 is applied, the numerical results for both the potential solution and the flux are considerably improved, even if only the first singular potential solution corresponding to Dirichlet–Neumann boundary conditions on $(-1, 1) \times \{0\}$ is removed, i.e., $L = 1$. The same pattern is observed if one continues to remove higher order singular potential solutions in the modified BEM, i.e., $L \in \{2, 3\}$, as can be seen from Fig. 3.

In order to describe quantitatively this phenomenon, define the normalized errors

$$err(u(\mathbf{x})) = \frac{|u_L^{(num)}(\mathbf{x}) - u^{(an)}(\mathbf{x})|}{\max_{\mathbf{y} \in \partial\tilde{\Omega}} |u^{(an)}(\mathbf{y})|}, \quad err(q(\mathbf{x})) = \frac{|q_L^{(num)}(\mathbf{x}) - q^{(an)}(\mathbf{x})|}{\max_{\mathbf{y} \in \partial\tilde{\Omega}} |q^{(an)}(\mathbf{y})|}, \tag{57}$$

for the potential solution and the flux, respectively, where $\partial\tilde{\Omega}$ denotes the set of the BEM nodes, since on using these errors divisions by zero and very high errors at points where the potential solution and/or the flux have relatively small values are avoided. Figs. 4(a) and (b) illustrate the normalized errors $err(u(\mathbf{x}))$ and $err(q(\mathbf{x}))$, respectively, on a semi-logarithmic scale for $\mathbf{x} \in (-1, 1) \times \{0\}$, obtained for various values of $L \in \{0, 1, 2, 3\}$. From these figures, as well as from Table 1 which presents the values of the normalized errors defined by Eq. (57) in the neighbourhood of the singular point $O = (0, 0)$, it can be seen the major effect in terms of accuracy of the modified BEM, namely a significant improvement in the accuracy of the numerical potential solution and flux from $O(10^{-1})$ to $O(10^{-15})$ for $err(u(\mathbf{x}))$ and from $O(10^{0})$ to $O(10^{-14})$ for $err(q(\mathbf{x}))$. As expected, the errors in the numerical flux are larger than the errors in the numerical potential solution due to the first order derivatives occuring in the representation of the flux.

Table 2 presents the numerical flux intensity factors, a_l, obtained for Example 1 with various $L \in \{1, 2, 3\}$. It can be seen from this table that the values obtained for the flux intensity factors for $l > 1$ are close to zero and this fact suggests that the singular potential solution $u_L^{(S)}(r, \theta)$ is dominated by its first term, $u_l^{(S)}(r, \theta)$ for $l = 1$. Hence, in the case of Example 1, it is sufficient to subtract only the first singular potential solution corresponding to Dirichlet–Neumann boundary

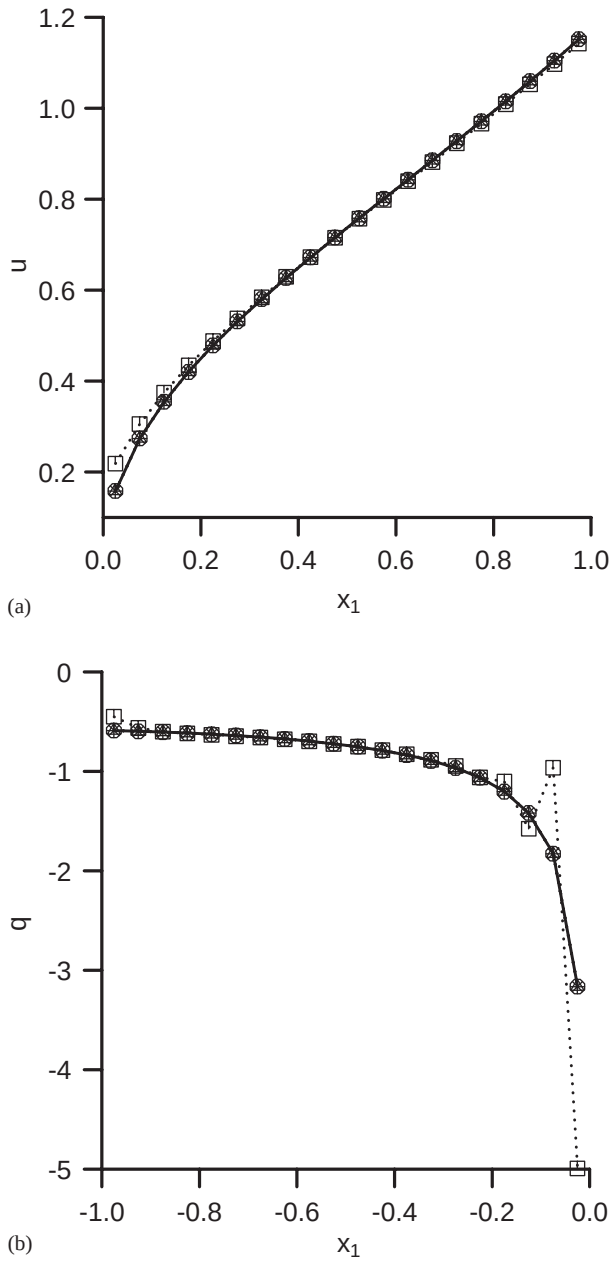

Fig. 3. (a) The analytical $u^{(an)}$ (—) and the numerical $u_L^{(num)}$ solutions on the boundary $(0,1) \times \{0\}$, and (b) the analytical $q^{(an)}$ (—) and the numerical $q_L^{(num)}$ fluxes on the boundary $(-1,0) \times \{0\}$, obtained with $N = 120$ boundary elements and by subtracting $L = 0$ $(\cdots \square \cdots)$, $L = 1$ $(\cdots \mathrm{O} \cdots)$, $L = 2$ $(\cdots \triangle \cdots)$ and $L = 3$ $(\cdots * \cdots)$ singular functions, for Example 1.

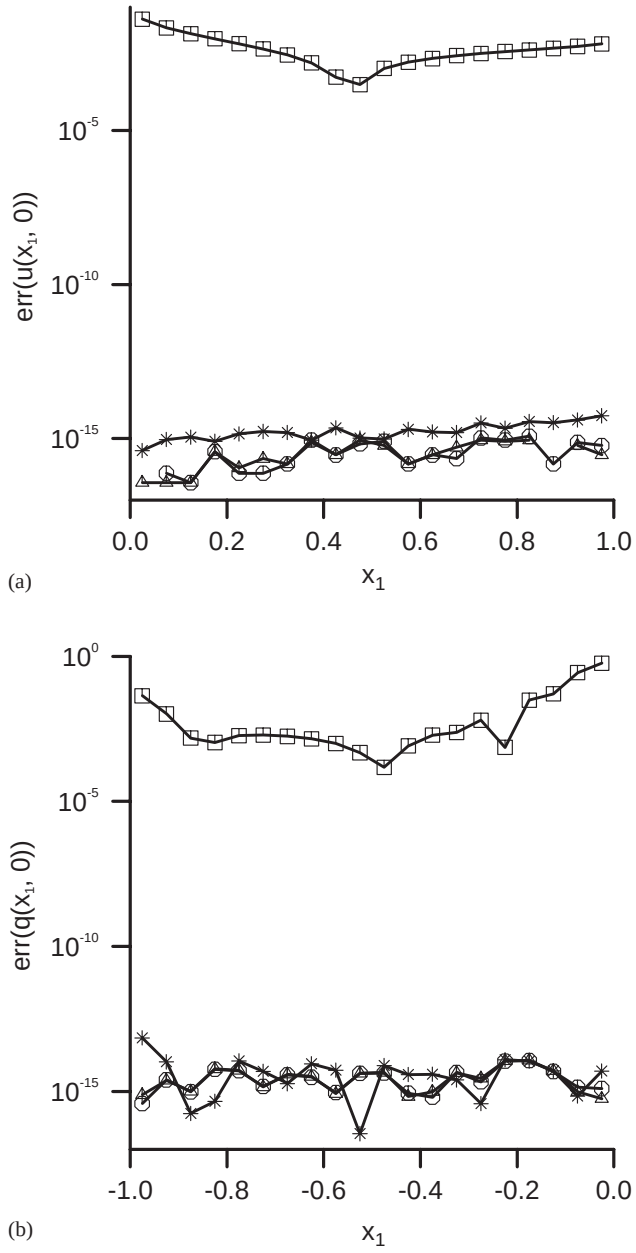

Fig. 4. The normalized errors (a) $err(u(\mathbf{x}))$ on the boundary $(0,1)\times\{0\}$, and (b) $err(q(\mathbf{x}))$ on the boundary $(-1,0)\times\{0\}$, on a semi-logarithmic scale, obtained with $N=120$ boundary elements and by subtracting $L=0$ $(-\square-)$, $L=1$ $(-\mathrm{O}-)$, $L=2$ $(-\triangle-)$ and $L=3$ $(-*-)$ singular functions, for Example 1.

conditions on $(-1,1)\times\{0\}$, i.e., $L=1$, in order to obtain very accurate numerical potential solution and flux. Although not presented here, it is reported that the numerical potential solution obtained on the remaining boundary of the domain Ω has the same accuracy as that presented on

Table 1
The values of the normalized error for the numerical solution $err(u_L(\mathbf{x}))$ and flux $err(q_L(\mathbf{x}))$, respectively, in the neighbourhood of the singular point $\mathbf{x} = (0,0)$ obtained with various L, for Example 1

$\mathbf{x}$	$err(q_0(\mathbf{x}))$	$err(q_1(\mathbf{x}))$	$err(q_2(\mathbf{x}))$	$err(q_3(\mathbf{x}))$
$(-0.225, 0.000)$	0.72×10^{-3}	0.11×10^{-13}	0.11×10^{-13}	0.12×10^{-13}
$(-0.175, 0.000)$	0.30×10^{-1}	0.11×10^{-13}	0.11×10^{-13}	0.11×10^{-13}
$(-0.125, 0.000)$	0.50×10^{-1}	0.49×10^{-14}	0.51×10^{-14}	0.51×10^{-14}
$(-0.075, 0.000)$	0.27×10^{0}	0.14×10^{-14}	0.98×10^{-15}	0.70×10^{-15}
$(-0.025, 0.000)$	0.57×10^{0}	0.12×10^{-14}	0.56×10^{-15}	0.50×10^{-14}
	$err(u_0(\mathbf{x}))$	$err(u_1(\mathbf{x}))$	$err(u_2(\mathbf{x}))$	$err(u_3(\mathbf{x}))$
$(0.025, 0.000)$	0.40×10^{-1}	0.26×10^{-15}	0.37×10^{-16}	0.41×10^{-15}
$(0.075, 0.000)$	0.21×10^{-1}	0.74×10^{-16}	0.37×10^{-16}	0.93×10^{-15}
$(0.125, 0.000)$	0.13×10^{-1}	0.37×10^{-16}	0.37×10^{-16}	0.11×10^{-14}
$(0.175, 0.000)$	0.93×10^{-2}	0.37×10^{-15}	0.37×10^{-15}	0.82×10^{-15}
$(0.225, 0.000)$	0.64×10^{-2}	0.74×10^{-16}	0.11×10^{-15}	0.14×10^{-14}

Table 2
The values of the flux intensity factors a_l obtained with $N = 120$ boundary elements and various L, for Example 1

L	a_1	a_2	a_3
1	0.17724×10^{1}	—	—
2	0.17724×10^{1}	0.12423×10^{-13}	—
3	0.17724×10^{1}	-0.14319×10^{-13}	0.95353×10^{-11}

the boundary adjacent to the singular point, thus approximating very accurately the analytical potential solution.

Both the second and the third examples investigated in this paper contain a singularity at the origin $O = (0,0)$ which is caused by a sharp corner in the boundary, as well as by the nature of the analytical potential solutions corresponding to these problems, i.e., the analytical potential solutions are given as linear combinations of the first four singular potential solutions satisfying homogeneous Dirichlet boundary conditions on the edges of the wedge. The analytical and the numerical fluxes on the boundaries $\{0\} \times (-1,0)$ and $(0,1) \times \{0\}$ obtained for Example 2 by subtracting $L \in \{0,1,2,3,4\}$ singular solutions are illustrated in Figs. 5(a) and (b), respectively. As expected, the numerical flux obtained using the standard BEM, i.e. $L = 0$, exhibits very high oscillations in the neighbourhood of the singular point and hence it represents an inaccurate approximation for the analytical flux. Moreover, from Fig. 5 it can be seen that oscillations in the numerical flux occur even far from the singularity, namely in the vicinity of the points $\mathbf{x} = (0,-1)$ and $(1,0)$. This problem can be overcome if instead of the standard BEM, the modified BEM described in the previous section is employed with $L \geqslant 1$. From Fig. 5 it can be noticed that the accuracy in the numerical flux is significantly improved even for $L = 1$ and a very good accuracy in the numerical flux on the boundary adjacent to the origin is attained as L approaches four, i.e., the number of singular solutions satisfying homogeneous Dirichlet boundary conditions on the edges of the wedge used in expression (53) for the analytical solution. A similar conclusion can be drawn from Table 3 which presents the normalized error for the flux in the neighbourhood of the

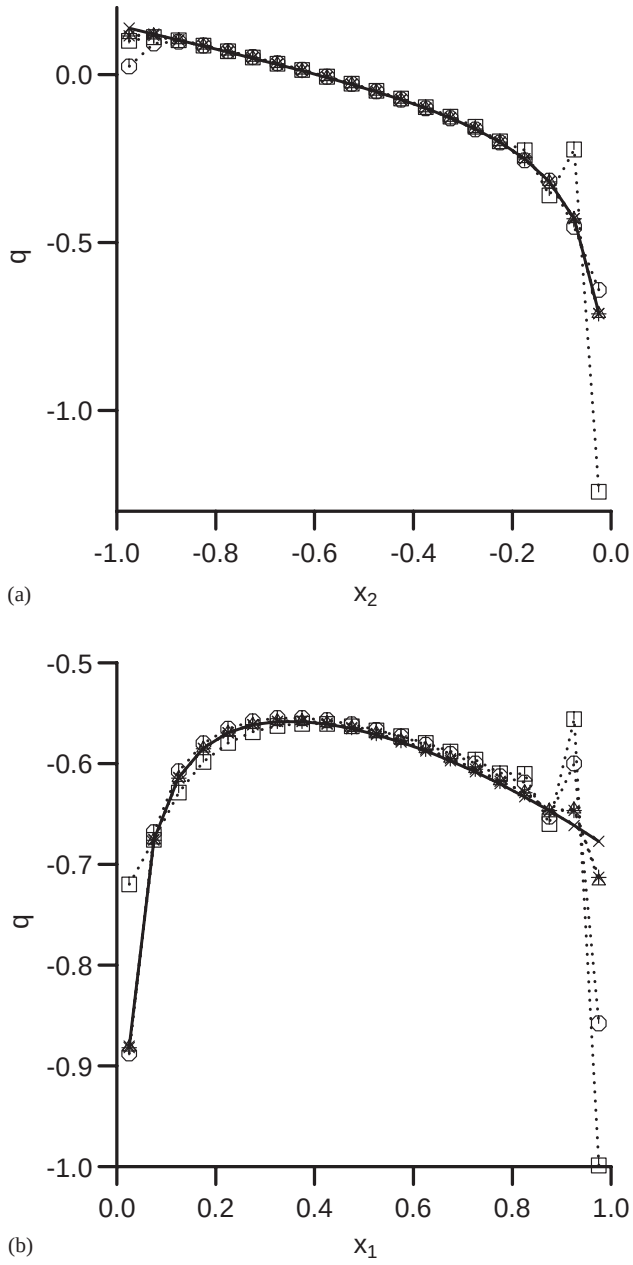

Fig. 5. The analytical $q^{(an)}$ (—-) and the numerical $q_L^{(num)}$ fluxes (a) on the boundary $\{0\} \times (-1, 0)$, and (b) on the boundary $(0, 1) \times \{0\}$, obtained with $N = 160$ boundary elements and by subtracting $L = 0$ $(-\square-)$, $L = 1$ $(-\mathrm{O}-)$, $L = 2$ $(-\triangle-)$, $L = 3$ $(-*-)$ and $L = 4$ $(-\times-)$ singular functions, for Example 2.

origin and, in addition, it can be seen from this table that the numerical flux in the vicinity of the singular point, obtained using the modified BEM with $L \geqslant 4$, is very accurate in comparison with its analytical value.

Table 3
The values of the normalized error for the numerical flux $err(q_L(\mathbf{x}))$ in the neighbourhood of the singular point $\mathbf{x} = (0,0)$ obtained with various L, for Example 2

$\mathbf{x}$	$err(q_0(\mathbf{x}))$	$err(q_1(\mathbf{x}))$	$err(q_2(\mathbf{x}))$	$err(q_3(\mathbf{x}))$	$err(q_4(\mathbf{x}))$	$err(q_5(\mathbf{x}))$
$(0.000, -0.225)$	0.42×10^{-2}	0.11×10^{-2}	0.22×10^{-1}	0.23×10^{-1}	0.75×10^{-12}	0.14×10^{-12}
$(0.000, -0.175)$	0.31×10^{-1}	0.46×10^{-2}	0.41×10^{-2}	0.45×10^{-2}	0.14×10^{-12}	0.15×10^{-13}
$(0.000, -0.125)$	0.45×10^{-1}	0.46×10^{-2}	0.58×10^{-3}	0.52×10^{-3}	0.19×10^{-13}	0.45×10^{-14}
$(0.000, -0.075)$	0.23×10^{0}	0.28×10^{-1}	0.19×10^{-2}	0.19×10^{-2}	0.63×10^{-13}	0.16×10^{-13}
$(0.000, -0.025)$	0.62×10^{0}	0.80×10^{-1}	0.23×10^{-2}	0.23×10^{-2}	0.80×10^{-13}	0.14×10^{-13}
$(0.025, 0.000)$	0.16×10^{0}	0.11×10^{-1}	0.20×10^{-2}	0.20×10^{-2}	0.73×10^{-13}	0.25×10^{-13}
$(0.075, 0.000)$	0.14×10^{-1}	0.70×10^{-2}	0.10×10^{-2}	0.11×10^{-2}	0.35×10^{-13}	0.11×10^{-13}
$(0.125, 0.000)$	0.26×10^{-1}	0.65×10^{-2}	0.55×10^{-3}	0.61×10^{-3}	0.33×10^{-13}	0.74×10^{-14}
$(0.175, 0.000)$	0.23×10^{-1}	0.53×10^{-2}	0.15×10^{-3}	0.21×10^{-3}	0.97×10^{-14}	0.14×10^{-13}
$(0.225, 0.000)$	0.18×10^{-1}	0.45×10^{-2}	0.18×10^{-3}	0.12×10^{-3}	0.16×10^{-13}	0.82×10^{-14}

Table 4
The values of the flux intensity factors a_l and the absolute error $Err(a_l)$ obtained with $N = 160$ boundary elements and various L, for Example 2

L	a_1	$Err(a_1)$	a_2	$Err(a_2)$	a_3	$Err(a_3)$	a_4	$Err(a_4)$
1	0.88089	0.11×10^{0}	—	—	—	—	—	—
2	0.99841	0.15×10^{-2}	−1.31168	0.11×10^{-1}	—	—	—	—
3	0.99855	0.14×10^{-2}	−1.31075	0.10×10^{-1}	−0.03971	0.39×10^{-2}	—	—
4	1.00000	0.52×10^{-13}	−1.30000	0.42×10^{-12}	0.00000	0.78×10^{-12}	−1.69999	0.34×10^{-10}
5	1.00000	0.16×10^{-13}	−1.30000	0.20×10^{-12}	0.00000	0.12×10^{-12}	−1.70000	0.85×10^{-11}

The absolute error for the flux intensity factors a_l, $1 \leqslant l \leqslant L$, can also be defined as

$$Err(a_l) = |a_l^{(num)} - a_l|, \quad 1 \leqslant l \leqslant L \tag{58}$$

in order to study the numerical retrieval of the flux intensity factors from a quantitative point of view. Table 4 presents the absolute errors $Err(a_l)$, $1 \leqslant l \leqslant 4$, as functions of the number L of singular solutions removed using the modified BEM, as well as the numerically retrieved flux intensity factors $a_l^{(num)}$ for $1 \leqslant l \leqslant 4$. From this table it can be concluded that the numerical flux intensities converge to their exact values as the number L of singular solutions subtracted increases, with the mention that the value $L = 4$ is sufficient in the case of Example 2 for obtaining very accurate numerical estimates for the flux intensity factors.

In Example 3 a singular BVP similar to that presented in Example 2 is analysed, but for the isotropic Hemholtz equation. Figs. 6(a) and (b) show the analytical and the numerical fluxes on the boundaries $\{0\} \times (-1, 0)$ and $(0, 1) \times \{0\}$, respectively, obtained for Example 3 when the standard BEM is employed, i.e., $L = 0$, as well as when the modified BEM is used, i.e., $L \in \{1, 2, 3, 4\}$. Also in this case, the numerical flux obtained when $L = 0$ is an inaccurate approximation for the analytical flux, at the same time giving rise to oscillations in the vicinity of the singular point $O = (0, 0)$. Again, this problem can be overcome by using the modified BEM presented in Section 4 and, consequently, the numerical flux $q_L^{(num)}$ approaches its analytical

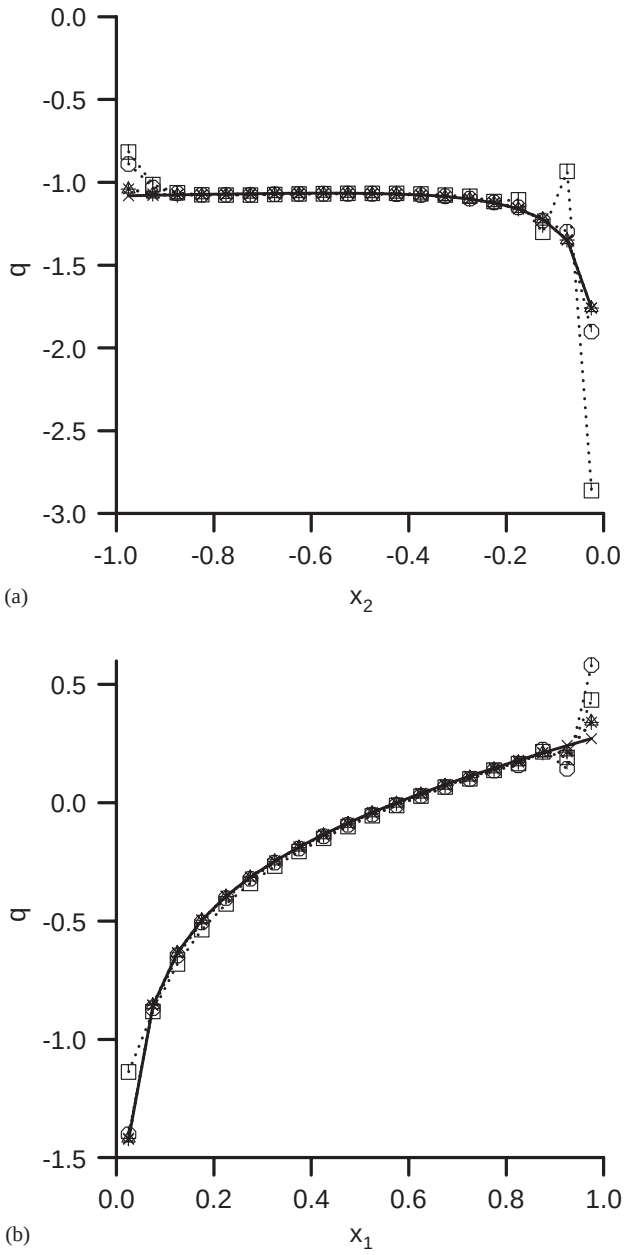

Fig. 6. The analytical $q^{(an)}$ (—) and the numerical $q_L^{(num)}$ fluxes (a) on the boundary $\{0\} \times (-1, 0)$, and (b) on the boundary $(0, 1) \times \{0\}$, obtained with $N = 160$ boundary elements and by subtracting $L = 0$ $(-\square-)$, $L = 1$ $(-\mathrm{O}-)$, $L = 2$ $(-\triangle-)$, $L = 3$ $(-*-)$ and $L = 4$ $(-\times-)$ singular functions, for Example 3.

value $q^{(an)}$ as L increases, as can be seen from Fig. 6, with the mention that $L \geqslant 4$ ensures very good numerical results for the flux not only far from the singularity, but also in its neighbourhood.

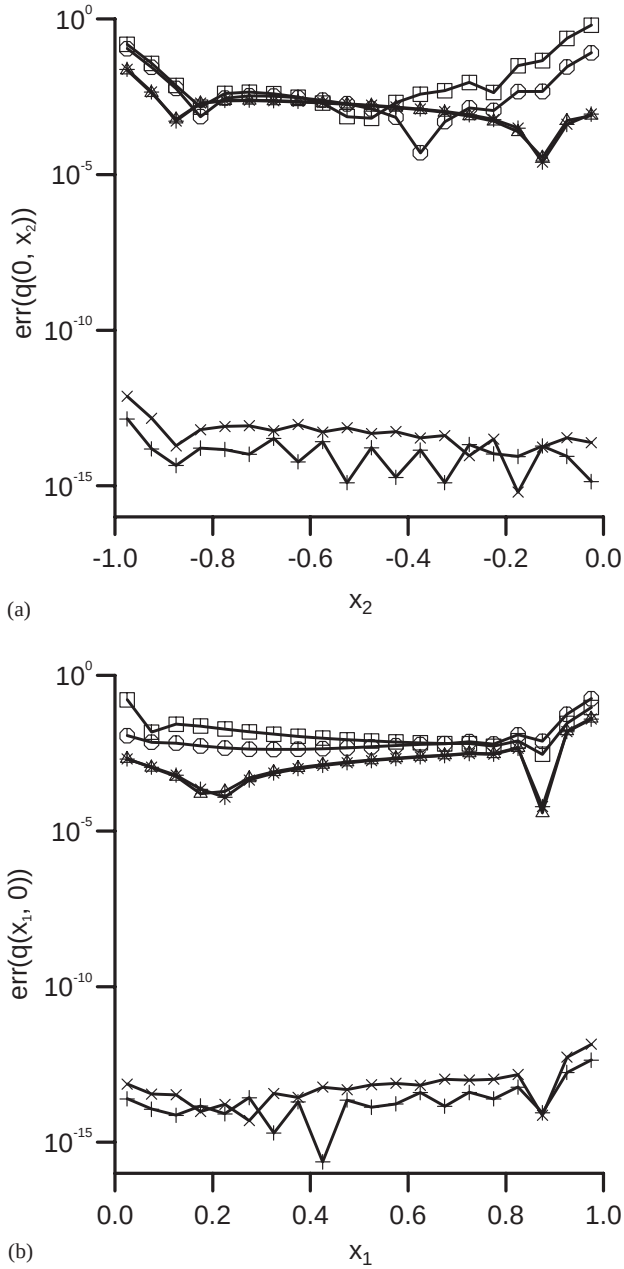

Fig. 7. The normalized error $err(q(\mathbf{x}))$ (a) on the boundary $\{0\} \times (-1, 0)$, and (b) on the boundary $(0, 1) \times \{0\}$, on a semi-logarithmic scale, obtained with $N = 160$ boundary elements and by subtracting $L = 0$ $(-\square-)$, $L = 1$ $(-\mathrm{O}-)$, $L = 2$ $(-\triangle-)$, $L = 3$ $(-*-)$, $L = 4$ $(-\times-)$ and $L = 5$ $(-+-)$ singular functions, for Example 3.

In Figs. 7(a) and (b) the normalized errors $err(q(\mathbf{x}))$ retrieved for $\mathbf{x} \in \{0\} \times (-1, 0)$ and $\mathbf{x} \in (0, 1) \times \{0\}$, respectively, when $L \in \{0, 1, 2, 3, 4\}$ singular solutions are subtracted are shown on a semi-logarithmic scale, whilst Table 5 presents their values obtained using the modified BEM in

Table 5
The values of the normalized error for the numerical flux $err(q_L(\mathbf{x}))$ in the neighbourhood of the singular point $\mathbf{x} = (0,0)$ obtained with various L, for Example 3

$\mathbf{x}$	$err(q_0(\mathbf{x}))$	$err(q_1(\mathbf{x}))$	$err(q_2(\mathbf{x}))$	$err(q_3(\mathbf{x}))$	$err(q_4(\mathbf{x}))$	$err(q_5(\mathbf{x}))$
$(0.000, -0.225)$	0.25×10^{-2}	0.12×10^{0}	0.23×10^{-1}	0.25×10^{-1}	0.56×10^{-12}	0.60×10^{-13}
$(0.000, -0.175)$	0.28×10^{-1}	0.31×10^{-1}	0.41×10^{-2}	0.46×10^{-2}	0.94×10^{-13}	0.28×10^{-15}
$(0.000, -0.125)$	0.46×10^{-1}	0.54×10^{-2}	0.79×10^{-3}	0.76×10^{-3}	0.23×10^{-13}	0.11×10^{-13}
$(0.000, -0.075)$	0.23×10^{0}	0.20×10^{-2}	0.20×10^{-2}	0.21×10^{-2}	0.49×10^{-13}	0.80×10^{-14}
$(0.000, -0.025)$	0.60×10^{0}	0.42×10^{-2}	0.23×10^{-2}	0.25×10^{-2}	0.62×10^{-13}	0.15×10^{-13}
$(0.025, 0.000)$	0.18×10^{0}	0.81×10^{-2}	0.15×10^{-2}	0.17×10^{-2}	0.46×10^{-13}	0.80×10^{-14}
$(0.075, 0.000)$	0.63×10^{-3}	0.81×10^{-2}	0.87×10^{-3}	0.10×10^{-2}	0.19×10^{-13}	0.10×10^{-13}
$(0.125, 0.000)$	0.17×10^{-1}	0.69×10^{-2}	0.49×10^{-3}	0.62×10^{-3}	0.59×10^{-14}	0.95×10^{-14}
$(0.175, 0.000)$	0.15×10^{-1}	0.54×10^{-2}	0.19×10^{-3}	0.31×10^{-3}	0.35×10^{-14}	0.40×10^{-14}
$(0.225, 0.000)$	0.11×10^{-1}	0.44×10^{-2}	0.64×10^{-4}	0.47×10^{-4}	0.50×10^{-14}	0.46×10^{-14}

Table 6
The values of the flux intensity factors a_l and the absolute error $Err(a_l)$ obtained with $N = 160$ boundary elements and various L, for Example 3

L	a_1	$Err(a_1)$	a_2	$Err(a_2)$	a_3	$Err(a_3)$	a_4	$Err(a_4)$
1	1.11546	0.11×10^{0}	—	—	—	—	—	—
2	1.00130	0.13×10^{-2}	−1.31168	0.11×10^{-1}	—	—	—	—
3	1.00111	0.11×10^{-2}	−1.30963	0.96×10^{-2}	−0.03033	0.30×10^{-1}	—	—
4	1.00000	0.32×10^{-13}	−1.30000	0.30×10^{-12}	0.00000	0.14×10^{-12}	−1.70000	0.24×10^{-10}
5	1.00000	0.11×10^{-14}	−1.30000	0.88×10^{-13}	0.00000	0.79×10^{-13}	−1.70000	0.12×10^{-11}

the vicinity of the origin. From both Fig. 7 and Table 5, it can be seen that the numerical flux converges to its analytical value as L increases, the value $L \geqslant 4$ is sufficient for retrieving very good numerical approximations for the flux and the modified BEM gives rise to numerical fluxes free of oscillations in the neighbourhood of the singular point $O = (0,0)$. In Table 6 is presented the absolute errors $Err(a_l)$, $1 \leqslant l \leqslant 4$, given by Eq. (58) and the numerical flux intensity factors $a_l^{(num)}$, $1 \leqslant l \leqslant 4$, obtained for Example 3 with various $L \in \{1,2,3,4,5\}$. From this table it can be noticed that the numerical flux intensities converge towards their exact values as L increases and the errors for these flux intensity factors are significantly improved for $L \geqslant 4$.

Overall, from the numerical results presented in this section it can be concluded that the modified BEM proposed in Section 4 is a very suitable method for solving BVPs exhibiting singularities caused by the presence of sharp corners in the boundary of the solution domain and/or abrupt changes in the boundary conditions, for both the Helmholtz and the modified Helmholtz equations in the isotropic case. The numerical potential solutions and fluxes retrieved using this singularity subtraction technique are very good approximations for their analytical values on the entire boundary, they are exempted from oscillations in the neighbourhood of the singular point and there is no need of further mesh refinement in the vicinity of the singularities. Although not illustrated numerically here, it should be noted that the proposed modified BEM

has given very accurate results for some other tested cases, including multiple singularity points and multiply connected domains for isotropic Helmholtz-type equations.

6. Conclusions

In this paper, the treatment of singularities in both isotropic and anisotropic Helmholtz-type equations has been investigated. The singular solutions corresponding to isotropic Helmholtz-type equations have been revised, whilst the singular solutions for the anisotropic case have been derived using an approach based on a change of variables which reduces the anisotropic Helmholtz-type equations to the canonical form with the same wave number. It has been shown that this method is suitable for overcoming the slow convergence rate for the standard BEM due to singularities caused by the presence of sharp corners in the boundary of the solution domain and/or the changes in the boundary conditions. Consequently, the standard BEM with constant elements has been modified in order to take account of the singularity, without an appreciable computational effort. The main advantages of this method, apart from those derived directly from the BEM, i.e., the discretization of the boundary only and the reduction of the dimension of the original problem are: (i) the considerable improvement in the accuracy of the numerical solution in the neighbourhood of the singular point, (ii) the reduced additional computational effort, (iii) the possibility of a straightforward implementation for other boundary elements, such as continuous linear, continuous quadratic, discontinuous linear and discontinuous quadratic boundary elements and (iv) further mesh refinement in the vicinity of the singularity is not necessary anymore. The method presented in this study and illustrated by three numerical examples can be easily and successfully applied to multiple singularity points and multiply connected domains, as well as to anisotropic Helmholtz-type equations, and it can be extended to the wave propagation in elastic isotropic and anisotropic corners, but these are deferred to future work.

Acknowledgements

The authors acknowledge the financial support received from the UK Royal Society. The very useful comments and suggestions made by Professor Federico París from the University of Seville and Professor Derek B. Ingham from the University of Leeds are also gratefully acknowledged.

References

[1] H. Motz, The treatment of singularities of partial differential equations by relaxation methods, *Quarterly Journal of Applied Mathematics* 4 (1946) 371–377.

[2] G.T. Symm, Treatment of singularities in the solution of Laplace's equation by an integral equation method, *NPL Report NAC 31*, 1973.

[3] R. Wait, Finite element methods for elliptic problems with singularities, *Computer Methods in Applied Mechanics and Engineering* 13 (1978) 141–150.

[4] D. Lesnic, L. Elliott, D.B. Ingham, Treatment of singularities in time dependent problems using the boundary element method, *Engineering Analysis with Boundary Elements* 16 (1995) 65–70.
[5] N.S. Mera, L. Elliott, D.B. Ingham, D. Lesnic, Singularities in anisotropic steady-state heat conduction using a boundary element method, *International Journal for Numerical Methods in Engineering* 53 (2002) 2413–2427.
[6] M. Elliotis, G. Georgiou, C. Xenophontos, The solution of Laplacian problems over L-shaped domains with a singular function boundary integral method, *Communications in Numerical Methods in Engineering* 18 (2002) 213–222.
[7] M.L. Williams, Stress singularities resulting from various boundary conditions in angular corners of plates in extension, *American Society of Mechanical Engineers Journal of Applied Mechanics* 19 (1952) 526–528.
[8] A. Portela, M.H. Aliabadi, D.P. Rooke, Efficient boundary element analysis of sharp notched plates, *International Journal for Numerical Methods in Engineering* 32 (1991) 445–470.
[9] J. Helsing, A. Jonsson, On the computation of stress fields on polygonal domains with V-notches, *International Journal for Numerical Methods in Engineering* 53 (2002) 433–453.
[10] M. Costabel, M. Dauge, Construction of corner singularities for Agmon–Douglis–Nirenberg elliptic systems, *Mathematische Nachrichten* 162 (1993) 209–237.
[11] J.R. Hutchinson, Vibration of plates, in: C.A. Brebbia (Ed.), *Boundary Elements X*, Springer, Berlin, 1988, pp. 415–430.
[12] D.E. Beskos, Boundary element method in dynamic analysis: Part II (1986–1996), *American Society of Mechanical Engineers Applied Mechanics Review* 50 (1997) 149–197.
[13] J.T. Chen, M.T. Liang, I.L. Chen, S.W. Chyuan, K.H. Chen, Dual boundary element analysis of wave scattering from singularities, *Wave Motion* 30 (1999) 367–381.
[14] J.T. Chen, K.H. Chen, Dual integral formulation for determining the acoustic modes of a two-dimensional cavity with a degenerate boundary, *Engineering Analysis with Boundary Elements* 21 (1998) 105–116.
[15] J.T. Chen, F.C. Wong, Dual formulation of multiple reciprocity method for the acoustic mode of a cavity with a thin partition, *Journal of Sound and Vibration* 217 (1998) 75–95.
[16] J.T. Chen, J.H. Lin, S.R. Kuo, W. Chyuan, Boundary element analysis for the Helmholtz eigenvalue problems with a multiply connected domain, *Proceedings of the Royal Society London* 457 (2001) 2521–2546.
[17] C. Huang, Z. Wu, R.D. Nevels, Edge diffraction in the vicinity of the tip of a composite wedge, *IEEE Transactions on Geoscience and Remote Sensing* 31 (1993) 1044–1050.
[18] I. Harari, P.E. Barbone, M. Slavutin, R. Shalom, Boundary infinite elements for the Helmholtz equation in exterior domains, *International Journal for Numerical Methods in Engineering* 41 (1998) 1105–1131.
[19] W.S. Hall, X.Q. Mao, A boundary element investigation of irregular frequencies in electromagnetic scattering, *Engineering Analysis with Boundary Elements* 16 (1995) 245–252.
[20] P.A. Barbone, J.M. Montgomery, O. Michael, I. Harari, Scattering by a hybrid asymptotic/finite element, *Computer Methods in Applied Mechanics and Engineering* 164 (1998) 141–156.
[21] A.D. Kraus, A. Aziz, J. Welty, *Extended Surface Heat Transfer*, Wiley, New York, 2001.
[22] M. Manzoor, D.B. Ingham, P.J. Heggs, The one-dimensional analysis of fin assembly heat transfer, *American Society of Mechanical Engineers Journal of Heat Transfer* 105 (1983) 646–651.
[23] A.S. Wood, G.E. Tupholme, M.I.H. Bhatti, P.J. Heggs, Steady-state heat transfer through extended plane surfaces, *International Communications in Heat and Mass Transfer* 22 (1995) 99–109.
[24] B. Schiff, Eigenvalues for ridged and other waveguides containing corners of angle $3\pi/2$ or 2π by the finite element method, *IEEE Transactions on Microwave Theory and Techniques* 39 (1991) 1034–1039.
[25] W. Cai, H.C. Lee, H.S. Oh, Coupling of spectral methods and the *p*-version for the finite element method for elliptic boundary value problems containing singularities, *Journal of Computational Physics* 108 (1993) 314–326.
[26] T.R. Lucas, H.S. Oh, The method of auxiliary mapping for the finite element solutions of elliptic problems containing singularities, *Journal of Computational Physics* 108 (1993) 327–342.
[27] X. Wu, H. Han, A finite-element method for Laplace- and Helmholtz-type boundary value problems with singularities, *SIAM Journal on Numerical Analysis* 134 (1997) 1037–1050.
[28] Y.S. Xu, H.M. Chen, Higher-order discretised boundary conditions at edges for TE waves, *IEEE Proceedings-Microwave Antennas and Propagation* 146 (1999) 342–348.

[29] V. Mantič, F. París, J. Berger, Singularities in 2D anisotropic potential problems in multi-material corners. Real variable approach, *International Journal of Solids and Structures* 40 (2003) 5197–5218.
[30] V. Mantič, F. París, On free terms and singular integrals in isotropic and anisotropic potential theory, in: S.N. Atluri, G. Yagawa, T.A. Cruse (Eds.), *Computational Mechanics '95*, Springer, Berlin, 1995, pp. 2806–2811.
[31] G. Chen, J. Zhou, *Boundary Element Methods*, Academic Press, London, 1992.
[32] C.A. Brebbia, J.C.F. Telles, L.C. Wrobel, *Boundary Element Techniques: Theory and Application in Engineering*, Springer, Berlin, 1984.
[33] L. Marin, L. Elliott, P.J. Heggs, D.B. Ingham, D. Lesnic, X. Wen, An alternating iterative algorithm for the Cauchy problem associated to the Helmholtz equation, *Computer Methods in Applied Mechanics and Engineering* 192 (2003) 709–722.
[34] L. Marin, L. Elliott, P.J. Heggs, D.B. Ingham, D. Lesnic, X. Wen, Conjugate gradient-boundary element solution for the Cauchy problem for Helmholtz-type equations, *Computational Mechanics* 31 (2003) 367–377.